

Analysis of Joint Transmit-Receive Diversity in Downlink MIMO Heterogeneous Cellular Networks

Ralph Tanbourgi, *Student Member, IEEE*, Harpreet S. Dhillon, *Member, IEEE*,
and Friedrich K. Jondral, *Senior Member, IEEE*

Abstract—We study multiple-input multiple-output (MIMO) based downlink heterogeneous cellular network (HetNets) with joint transmit-receive diversity using orthogonal space-time block codes at the base stations (BSs) and maximal-ratio combining (MRC) at the users. MIMO diversity with MRC is especially appealing in cellular networks due to the relatively low hardware complexity at both the BS and user device. Using stochastic geometry, we develop a tractable stochastic model for analyzing such HetNets taking into account the irregular and multi-tier BS deployment. We derive the coverage probability for both interference-blind (IB) and interference-aware (IA) MRC as a function of the relevant tier-specific system parameters such as BS density and power, path loss law, and number of transmit (Tx) antennas. Important insights arising from our analysis for typical HetNets are for instance: (i) IA-MRC becomes less favorable than IB-MRC with Tx diversity due to the smaller interference variance and increased interference correlation across Rx antennas; (ii) ignoring spatial interference correlation significantly overestimates the performance of IA-MRC; (iii) for small number of Rx antennas, selection combining may offer a better complexity-performance trade-off than MRC.

Index Terms—MIMO, space-time coding, maximal-ratio combining, coverage probability, Poisson point process.

I. INTRODUCTION

NETWORK densification and multiple-input multiple-output (MIMO) communications are two promising approaches to address the ever-increasing rate and coverage demands in cellular systems [2]. Network densification is realized by opportunistically deploying a variety of tiers of low-power base stations (BSs) inside the existing network, e.g., to serve high-traffic areas within macro cells, thereby rendering the network increasingly *heterogeneous*. MIMO, on the other hand, can improve reliability and/or link spectral efficiency by leveraging the spatial degrees-of-freedom in fading channels. Due to the fundamental shift associated with heterogeneous cellular networks (HetNets), MIMO and HetNets cannot be analyzed in isolation; many characteristics unique to HetNets, most notably multi-tier deployment, limited site-planning, and heterogeneous parametrization, clearly influence the channel “seen” by a typical multi-antenna receiver. Understanding this interplay, however, is challenging and renders a comprehensive

analysis of MIMO in HetNets difficult. This paper addresses this challenge by developing a tractable model, which allows studying the performance of MIMO diversity in HetNets.

A. Motivation and Related Work

MIMO techniques can be open-loop or closed-loop based. Closed-loop techniques, such as spatial-multiplexing or multi-user MIMO, have been the focus of many works on MIMO cellular networks, see for instance [3]–[6], and the references therein. These works demonstrate that closed-loop MIMO schemes can achieve considerable gains over conventional communications systems when channel state information at the transmitter (CSI-T) is available. Reliable CSI-T, however, may not always be available in practice, e.g., in high mobility scenarios [7]. In such cases, open-loop techniques, requiring CSI only at the receiver (CSI-R), have to be used instead. For instance, the 3rd Generation Partnership Program (3GPP) Long Term Evolution (LTE) standard supports different open-loop modes since release 8; for example, transmission mode 2 uses a space-frequency block code (SFBC) to offer transmit diversity over two or four transmit (Tx) antennas [8]. On the mobile receiver side, space and complexity limitations typically preclude a large number of receive (Rx) antennas—oftentimes not exceeding two or four antennas—and allow only for simple linear combining schemes. One such combining scheme is maximal-ratio combining (MRC), which offers a good trade-off between performance and complexity, and is therefore ubiquitously found in multi-antenna consumer devices. Especially in the context of MIMO communications, MRC may sometimes be even more appealing than interference-canceling receivers, since the latter require accurate knowledge of the other-cell interference signals, which is harder to realize when multiple Tx antennas are active [9].

Depending on how interference is treated at the combining stage, one can distinguish between two types of MRC, namely *interference-blind* (IB) and *interference-aware* (IA) MRC. The former—and more popular—ignores the interference experienced at each Rx antenna. The combiner coefficients then follow from the well-known channel matched-filter approach [9]. IA-MRC, in contrast, takes the interference into account though still treating it as white noise. More specifically, the interference power experienced at each antenna within one coherence period or block/frame is measured and interpreted as additional receiver noise. Following the original MRC approach from [10], the optimal combiner weights are then computed taking into account the (possibly unequal) interference-

R. Tanbourgi and F. K. Jondral are with the Communications Engineering Lab (CEL), Karlsruhe Institute of Technology (KIT), Germany. Email: {ralph.tanbourgi, friedrich.jondral}@kit.edu.

H. S. Dhillon is with the Wireless@VT, Department of ECE, Virginia Tech, Blacksburg, VA, USA. Email: hdhillon@vt.edu.

This work was submitted in part to the IEEE International Conference on Communications 2015, London, UK [1].

plus-noise power levels at the Rx antennas. Measuring the per-antenna interference power can be achieved within the channel estimation phase, e.g., by decoding also the cell-specific reference symbols from interfering BSs or by using techniques from [11], [12]. Both types of MRC are well-understood for networks with fixed geometry, see for instance [10], [13]–[15], and recently also for networks with dynamic/varying geometry [16]–[19]. IA-MRC was also studied for single-tier single-Tx antenna cellular networks with one Tx antenna in [20].

In the context of downlink HetNets, MIMO diversity with MRC is not yet well-understood, since prior works on single-tier networks do not directly apply due to the specific nature of the interference governing these networks. One interesting question, for instance, is whether the performance gain of IA-MRC over IB-MRC justifies the (slight) increase in complexity in a typical downlink MIMO HetNet setting. Furthermore, how sensitive is their relative performance to the number of Tx and Rx antennas? And how does spatial interference correlation across Rx antennas affect the performance of MRC?

Certainly, extensive system-level simulations cannot be the solution to address the above questions since they usually offer only limited insights and fail to reveal dependencies among system parameters. As a viable alternative approach to simulations, spatial modeling using stochastic geometry [21] has gained much attention recently, which resulted in a number of notable works, see for instance [22]–[28] and the references therein. In order to properly assess the performance of MIMO diversity with MRC in downlink HetNets and to obtain a better understanding of the trade-offs involved, a similar spatial model and meaningful analysis is therefore required. This is the main contribution in this work.

B. Contributions and Outcomes

In this work, we study the coverage performance of downlink HetNets with MIMO diversity, where users employ IB-MRC or IA-MRC. Our main contributions are outlined below.

Analytical model: In Section II, we develop a tractable stochastic model for downlink MIMO diversity with orthogonal space-time block codes (OSTBCs) and IB-MRC/IA-MRC. To reflect the irregular and multi-tier deployment of BSs found in practice, we use a Poisson point process (PPP) to model the BS locations of a K -tier HetNet. The model captures relevant tier-specific parameters, such as BS density and Tx power, path loss exponent, and number of Tx antennas. Based on this model, we then derive the coverage probability for both types of MRC in Section IV. For IA-MRC, we focus on the case with two Rx antennas. The theoretic expressions can be evaluated easily using standard numerical software, while in certain cases they can be further simplified analytically.

Second-order statistics of HetNet interference: In Section III, we study the interference power (hereafter, simply *interference*) dynamics at a multi-antenna receiver in HetNets, thereby complementing earlier work, which focused on ad hoc networks [26]. Interference dynamics affect the performance of interference-aware diversity combining schemes such as IA-MRC. Our analysis shows that the interference variance measured at a typical user is tier-independent when the path

loss exponent and the number of Tx antennas is equal in each tier. It monotonically decreases with the path loss exponent. In direct comparison with the literature, our analysis indicates that the interference variance is smaller in HetNets than in ad hoc networks, where interferers can be much closer to a receiver. Moreover, the gains of interference-aware diversity combining are expected to decrease when adding more active Tx antennas since interference variance then becomes smaller.

Interestingly, the interference correlation across antennas of a typical user is independent from the tier with which this user associates. When the number of Tx antennas is equal in each tier, the correlation becomes entirely tier-independent. In this case, the correlation coefficient is an increasing univariate function of the number of active Tx antennas. In line with the effect of decreasing interference variance explained above, the gains of interference-aware diversity combining are expected to decrease when adding more active Tx antennas due to the higher interference correlation across Tx antennas.

Design Insights: In Section V, we discuss the theoretic results developed in the prior sections using numerical examples.

In a typical three-tier MIMO scenario with IB-MRC at the receivers, the gain of doubling the number of Rx antennas is roughly 2.5 dB at operating points of practical relevance. For IA-MRC, this gain is roughly 3.6 dB. Adding more Tx antennas has only a minor impact on the performance of IA-MRC; the coverage probability improvement by adding a second Tx antenna is less than 5%. Relative to IB-MRC, IA-MRC improves performance only slightly with descending trend as the number of Tx antennas increases. This trend is due to the higher interference correlation across Rx antennas resulting from the interference-smoothing effect of Tx diversity. The coverage probability improvement of 1×2 SIMO over SISO transmission in the practical regime is between 12%–66% for IB-MRC, while an additional small improvement of 1%–3% is obtained by IA-MRC. Although interference power estimation needed in IA-MRC can be realized with affordable complexity, the outcome of this comparison suggests that IA-MRC is less favorable than IB-MRC in MIMO HetNets with Tx diversity.

Spatial interference correlation across Rx antennas, caused by the common locations of interfering BSs, influences the performance of IA-MRC and should not be ignored in the analysis; ignoring it leads to a significantly optimistic performance characterization. In contrast, assuming full correlation underestimates the true performance by no more than 2% for the same setting. Moreover, it is shown that assuming full correlation in IA-MRC is equivalent to IB-MRC. Interestingly, it does not matter for the diversity order of IA-MRC if one assumes no correlation or full correlation of the interference.

As a byproduct of the comparison of MRC with selection combining (SC), we extend prior work by deriving the coverage probability of SC for SIMO HetNets. Our comparison indicates that the gains of both IA-MRC and IB-MRC over SC are relatively low when the number of Rx antennas is small (around 10–15%). In this regime, the increased complexity associated with MRC might outweigh the obtainable improvement over SC in HetNets. When doubling the number of Rx antennas, the improvement is around 25%–35%, thereby revealing a sublinear increase with the number of Rx antennas.

Notation: We use sans-serif-style letters (z) for denoting random variables and serif-style letters (z) for denoting their realizations or variables. We define $(z)^+ \triangleq \max\{0, z\}$.

II. SYSTEM MODEL

A. Network Geometry and User Association

We consider a K -tier HetNet in the downlink with BSs irregularly scattered in the plane, see Fig. 1. We model the irregular BS locations in tier k by an independent stationary planar PPP Φ_k with density λ_k . We denote by $\Phi \triangleq \cup_{k=1}^K \Phi_k$ the entire set of BSs. The spatial Poisson model is widely-accepted for analyzing (multi-tier) cellular networks [22]–[24], and recently also MIMO HetNets [5], [6]. All BSs in tier k transmit an OSTBC using M_k antennas. Similarly, we assume that mobile receivers (users) are equipped with N antennas. The users are independently distributed on the plane according to some stationary point process. By Slivnyak's Theorem [21] and due to the stationarity of Φ , we can focus the analysis on a *typical* user located at the origin $o \in \mathbb{R}^2$. BSs in tier k transmit with total power P_k , which is equally divided across all active Tx antennas. At the typical user, the long-term received power from a tier k BS located at $\mathbf{x}_i \in \Phi_k$ is thus $P_k \|\mathbf{x}_i\|^{-\alpha_k}$, where $\|\cdot\|^{-\alpha_k}$ is the distance-dependent path loss with path loss exponent $\alpha_k > 2$. We assume independent and identically distributed frequency-flat Rayleigh fading. Table I summarizes frequently recurring notation used in this work.

Users are assumed to associate with the BS providing the strongest average measured received power, which is a common assumption in cellular systems. Note that this association rule is generally not coverage maximizing in MIMO HetNets with unequal M_k and requires a *biased* association rule, see [6] for more details. Including biasing in the model, e.g., using similar techniques as in [6], [23], is left for possible future work. For the typical user, the serving BS is hence the one maximizing $P_k \|\mathbf{x}_i\|^{-\alpha_k}$. Without loss of generality, we label the location of this BS by \mathbf{x}_o and denote by $y \triangleq \|\mathbf{x}_o\|$ its distance to the typical user. For convenience, we define $\Phi^o \triangleq \Phi \setminus \{\mathbf{x}_o\}$ (similarly, $\Phi_k^o \triangleq \Phi_k \setminus \{\mathbf{x}_o\}$), i.e., the set of interfering BSs. From the association rule discussed above it follows that, given $y = y$ and that the serving BS is from tier ℓ , Φ_k^o is a homogeneous PPP on $\mathbb{R}^2 \setminus b(0, d_k)$, where $d_k = \hat{P}_k^{1/\alpha_k} y^{1/\hat{\alpha}_k}$ with $\hat{P}_k \triangleq P_k/P_\ell$ and $\hat{\alpha}_k \triangleq \alpha_k/\alpha_\ell$.

It will be useful in the later analysis to know the probability that a user associates with a certain tier k as well as the conditional probability density function (PDF) of the distance to the serving BS, which are given in the following lemma.

Lemma 1 (Association Probability and Distance PDF [23]). *A user associates with the ℓ -th tier with probability*

$$A_\ell = 2\pi\lambda_\ell \int_0^\infty y \exp\left(-\pi \sum_{k=1}^K \lambda_k \hat{P}_k^{2/\alpha_k} y^{2/\hat{\alpha}_k}\right) dy. \quad (1)$$

The PDF of the distance $y \triangleq \|\mathbf{x}_o\|$ to the serving BS, given that it belongs to tier ℓ , is

$$f_{y,\ell}(y) = \frac{2\pi\lambda_\ell y}{A_\ell} \exp\left(-\pi \sum_{k=1}^K \lambda_k \hat{P}_k^{2/\alpha_k} y^{2/\hat{\alpha}_k}\right), \quad y \geq 0. \quad (2)$$

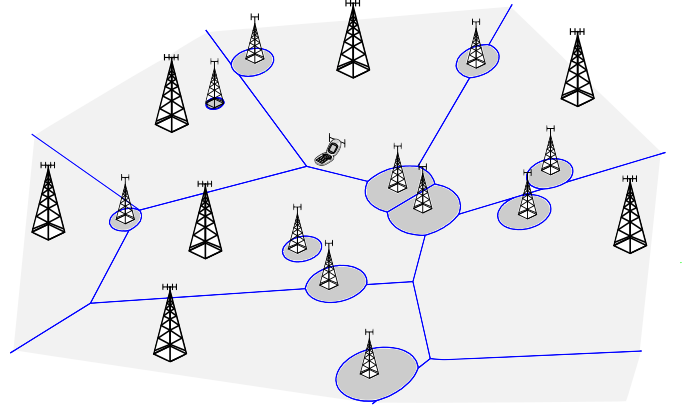


Fig. 1. Example: Downlink HetNet with $K = 2$. Tier-1 (macro) BSs have 4 antennas Tier-2 (small-cell) BSs have 2 antennas. Typical user has 2 antennas.

B. OSTBC MIMO Signal Model

All BSs in tier k use an (M_k, T_k, r_k) -OSTBC, where $T_k \geq 1$ is the codeword length and $r_k \in (0, 1]$ is the code rate; T_k can be seen as the number of slots for conveying $S_k = T_k r_k$ symbols using M_k Tx antennas. For analytical tractability, we shall consider only *power-balanced* (M_k, T_k, r_k) -OSTBCs, i.e., having the property that exactly S_k symbols are transmitted, or equivalently that $S_k \leq M_k$ antennas are active, in every slot. This will allow us to assign a constant power load of P_k/S_k to every symbol-antenna pair in every slot. Practical examples of balanced OSTBCs are for instance $(1, 1, 1)$ (single-antenna), $(2, 2, 1)$ (Alamouti), $(4, 4, 1/2)$, and $(4, 4, 3/4)$, see [29], [30]. We use the notation $\mathbf{v}_{i,\tau} \in \{0, 1\}^{M_k \times 1}$ to indicate the active antennas of BS i in slot τ , i.e., the m -th entry of $\mathbf{v}_{i,\tau}$ is one if antenna m is active and zero otherwise.

Assume for the moment that the typical user associates with the ℓ -th tier. It will then be served by an (M_ℓ, T_ℓ, r_ℓ) -OSTBC. The interference-plus-noise corrupted received signal at the typical user in slot $\tau \in [1, \dots, T_\ell]$ can then be expressed by the $N \times 1$ vector

$$\mathbf{y}_\tau = \mathbf{H}_o \mathbf{c}_{o,\tau} + \sum_{k=1}^K \sum_{i \in \Phi_k^o} \mathbf{H}_i \mathbf{c}_{i,\tau} + \mathbf{n}_\tau, \quad (3)$$

where

- $\mathbf{H}_i \in \mathbb{C}^{N \times M_k}$ is the channel matrix describing the fading between the i -th BS of the k -th tier and the typical user. The elements of \mathbf{H}_i , $h_{i,nm}$, are $\mathcal{CN}(0, 1)$ distributed and remain constant over one codeword. We assume $\mathbb{E}[h_{i,nm} h_{j,uv}^*] = 0$ unless $i = j$, $n = u$, and $m = v$.
- $\mathbf{c}_{i,\tau} \in \mathbb{C}^{M_k \times 1}$ is a vector consisting of the space-time coded symbols of the i -th BS sent from the $S_k \leq M_k$ active antennas in slot τ and received with average signal strength $\sqrt{P_k/S_k} \|\mathbf{x}_i\|^{\alpha_k}$. We assume independent emissions across BSs, i.e., $\mathbb{E}[\mathbf{c}_i \mathbf{c}_j^H] = 0$ for all $i \neq j$. It is reasonable to assume also that $\mathbb{E}[\mathbf{c}_{i,\tau}] = 0$ element-wise and $\mathbb{E}[\mathbf{c}_{i,\tau} \mathbf{c}_{i,\tau}^H] = P_k/S_k \|\mathbf{x}_i\|^{\alpha_k} \text{diag}(\mathbf{v}_{i,\tau})$, where $\text{diag}(\mathbf{v}_{i,\tau})$ is a diagonal matrix with entries $\mathbf{v}_{i,\tau}$. The latter assumption follows from the *balanced-power* property of the considered OSTBCs.

TABLE I
NOTATION USED IN THIS WORK

Notation	Description
$\Phi_k; \lambda_k$	PPP describing the BS locations in tier k ; average density of tier- k BSs; $\Phi \triangleq \cup_{k=1}^K \Phi_k$
P_k	BS transmit power in tier k
α_k	Path loss exponent in tier k
$N; M_k$	Number Rx antennas at the typical user; number of Tx antennas per BS in tier k
$\mathbf{H}_i; \mathbf{h}_{i,nm}$	$N \times M_k$ channel matrix between typical user and i -th tier k BS; entries of \mathbf{H}_i from $\mathcal{CN}(0, 1)$
σ^2	Receiver noise (AWGN) power
(M_k, T_k, r_k)	OSTBC with codeword length T_k , code rate r_k , and M_k Tx antennas
S_k	Number of symbols encoded in an (M_k, T_k, r_k) -OSTBC; number of active Tx antennas per slot
$\mathbf{A}_{nm}, \mathbf{B}_{nm}$	Dispersion matrices characterizing an OSTBC
$\mathbf{l}_n; \mathbf{l}_{i,\text{eqv}}$	Interference power at the n -th antenna; interference from i -th BS after diversity combining
$\overline{\text{SNR}}_\ell(y)$	Mean SNR from a serving ℓ -th tier BS at distance y
$\text{SINR}_\ell(y)$	SINR from a serving ℓ -th tier BS at distance y
SINR	SINR at the typical user
T	Target SINR
P_c	Coverage probability $\mathbb{P}(\text{SINR} > T)$

- $\mathbf{n}_\tau \in \mathbb{C}^{N \times 1}$ is a vector describing the receiver noise with independent $\mathcal{CN}(0, \sigma^2)$ entries.

Upon receiving all T_ℓ code symbols corresponding to one codeword, the typical user stacks the vectors $\mathbf{y}_1, \dots, \mathbf{y}_{T_\ell}$ to form a new $NT_\ell \times 1$ vector

$$\bar{\mathbf{y}} = \begin{bmatrix} \mathbf{H}_o \mathbf{c}_{o,1} \\ \vdots \\ \mathbf{H}_o \mathbf{c}_{o,T_\ell} \end{bmatrix} + \sum_{k=1}^K \sum_{i \in \Phi_k^o} \underbrace{\begin{bmatrix} \mathbf{H}_i \mathbf{c}_{i,1} \\ \vdots \\ \mathbf{H}_i \mathbf{c}_{i,T_\ell} \end{bmatrix}}_{\bar{\mathbf{i}}_i} + \begin{bmatrix} \mathbf{n}_1 \\ \vdots \\ \mathbf{n}_{T_\ell} \end{bmatrix}, \quad (4)$$

where $\bar{\mathbf{i}}_i \in \mathbb{C}^{NT_\ell \times 1}$ is the interference signal from the i -th BS received over the entire codeword period. With CSI at the receiver, $\bar{\mathbf{y}}$ is linearly processed/combined to form a decision variable. Two types of MRC are considered, which differ in the amount of required CSI. More specifically, IB-MRC requires knowledge of \mathbf{H}_o , while IA-MRC requires knowledge of \mathbf{H}_o and of the interference power. The squared Frobenius norm of a matrix $\mathbf{X} \in \mathbb{C}^{U \times V}$ is given by $\|\mathbf{X}\|_F^2 = \sum_{u=1}^U \sum_{v=1}^V |x_{uv}|^2$. The following lemma will be useful in the later analysis.

Lemma 2 (Gaussian Matrices). *Let the matrix $\mathbf{X}(u) \in \mathbb{C}^{v \times w}$ have $u \leq vw$ $\mathcal{CN}(0, 1)$ -distributed entries and $vw - u$ zeros. Then $\|\mathbf{X}(u)\|_F^2$ is Erlang distributed with distribution function*

$$\mathbb{P}(\|\mathbf{X}(u)\|_F^2 \leq \theta) = 1 - e^{-\theta} \sum_{j=0}^{u-1} \frac{\theta^j}{j!}. \quad (5)$$

and p -th (raw) moment

$$\mathbb{E} [\|\mathbf{X}(u)\|_F^{2p}] = \frac{\Gamma(u+p)}{\Gamma(u)}, \quad p > -u. \quad (6)$$

It is known that the performance of diversity-combining schemes is influenced by the second-order properties of the interference dynamics, as reported in [26]–[28] for the ad hoc network model. Next, we analyze the second-order statistics of the interference in MIMO HetNets.

III. SECOND-ORDER STATISTICS OF HETNET INTERFERENCE

The performance of diversity combining is fundamentally limited by the nature of the channel observed by the receiver. More specifically, variability of the reception quality on the one hand, and degree of their correlation across antennas on the other, dictate how much can be gained by such techniques. Clearly, if the reception quality fluctuates considerably and independently across antennas, large gains can be expected. If, in contrast, the channel quality remains the same or does not vary significantly across antennas, little to no gains can be expected. From (3) it is evident that the resulting per-antenna reception quality is not only affected by the fading on the desired link but also by interference. Being a dynamic quantity, the latter contributes to the overall correlation structure and variability of the reception quality with its own statistical properties. Compared to the influence from the desired channel, this contribution is yet relatively unexplored, particularly within the context of HetNets. This motivates to take a closer look at the second-order characteristics of the interference experienced at the typical user.

Let $\mathbf{h}_{i,n} = [\mathbf{h}_{i,n1}, \dots, \mathbf{h}_{i,nM_k}]$ be the n -th row of \mathbf{H}_i . Then, the interference (power) in slot τ (we shall drop the index τ in the following) measured at the n -th antenna, averaged over the code symbols \mathbf{c}_i in one frame, is

$$\begin{aligned} \mathbf{l}_n &= \mathbb{E}_{\mathbf{c}_i} \left[\left(\sum_{k=1}^K \sum_{i \in \Phi_k^o} \mathbf{h}_{i,n} \mathbf{c}_i \right) \left(\sum_{k=1}^K \sum_{i \in \Phi_k^o} \mathbf{h}_{i,n} \mathbf{c}_i \right)^H \right] \\ &\stackrel{(a)}{=} \sum_{k=1}^K \sum_{i \in \Phi_k^o} \mathbf{h}_{i,n} \mathbb{E} [\mathbf{c}_i \mathbf{c}_i^H] \mathbf{h}_{i,n}^H \\ &\stackrel{(b)}{=} \sum_{k=1}^K \sum_{i \in \Phi_k^o} \frac{P_k}{S_k \|\mathbf{x}_i\|^{\alpha_k}} \mathbf{h}_{i,n} \text{diag}(\mathbf{v}_{i,\tau}) \mathbf{h}_{i,n}^H \\ &= \sum_{k=1}^K \sum_{i \in \Phi_k^o} \frac{P_k}{S_k \|\mathbf{x}_i\|^{\alpha_k}} \|\mathbf{h}_{i,n}(S_k)\|_F^2 = \sum_{k=1}^K \mathbf{l}_{n,k}, \end{aligned} \quad (7)$$

where (a) follows from the independence between the \mathbf{c}_i across BSs and (b) follows from the correlation properties of the \mathbf{c}_i .

A. Normalized Interference Variance

Combining (7) and (3) we can see that the dynamic part not belonging to the fading on the desired channel is $\mathbf{l}_n + \sigma^2$. Since this term is essentially a function of the long-term received useful power $P_\ell y^{-\alpha_\ell}$ through the cell association rule, it is reasonable to consider the normalized version

$(I_n + \sigma^2)/(P_\ell y^{-\alpha_\ell}) \triangleq I'_n$. This expression can be intuitively understood as the interference-to-average-signal ratio in branch n . Given that the serving BS is at distance y and belongs to tier ℓ , the corresponding conditional variance seen by the typical user is

$$\begin{aligned} \text{Var}_{\ell,y}[I'_n] &\stackrel{(a)}{=} \frac{y^{2\alpha_\ell}}{P_\ell^2} \sum_{k=1}^K \text{Var}_{\ell,y}[I_{n,k}] \\ &\stackrel{(b)}{=} 2\pi y^{2\alpha_\ell} \sum_{k=1}^K \hat{P}_k^2 \lambda_k \frac{\mathbb{E}[\|\mathbf{h}_n(S_k)\|_F^4]}{S_k^2} \int_{d_k}^{\infty} r^{-2\alpha_k+1} dr \\ &\stackrel{(c)}{=} \pi \sum_{k=1}^K \frac{\lambda_k \hat{P}_k^{2/\alpha_k}}{\alpha_k - 1} \left(1 + \frac{1}{S_k}\right) y^{2/\alpha_k}, \end{aligned} \quad (8)$$

where (a) follows from the fact $\text{Var}[z + c] = \text{Var}[z]$ and from the independence of the $I_{n,k}$ across tiers, (b) follows from Campbell's theorem [21] and from the radius d_k of the exclusion ball for the k -th tier due to the cell association rule, and (c) follows from Lemma 2. The expression in (8) reflects the variance of the normalized interference for a specific user location relative to the network. We thus still need to decondition on y and the associated tier ℓ , which can be done using Lemma 1. To obtain a more tractable expression that reveals the underlying trend, we shall assume equal path loss exponents and the same number of active antennas across tiers, i.e., $\alpha_k \equiv \alpha$ and $S_k \equiv S$, next. The variance experienced at the typical user then becomes

$$\begin{aligned} \text{Var}[I'_n] &= \sum_{\ell=1}^K 2\pi \lambda_\ell \int_0^{\infty} y \text{Var}_{\ell,y}[I'_n] \\ &\quad \times \exp\left(-\pi y^2 \sum_{k=1}^K \lambda_k \hat{P}_k^{2/\alpha}\right) dy = \frac{1 + \frac{1}{S}}{\alpha - 1}. \end{aligned} \quad (9)$$

The following observations can be made from (9):

- Interestingly, the variance of the normalized interference at the typical user neither depends on the number of tiers nor on their parameters P_k and λ_k when $\alpha_k \equiv \alpha$. This result is consistent with [23], [24], where the independence between the SINR distribution and the number/parameters of tiers was shown for equal α_k and absence of noise.
- In line with our intuition, the interference variance increases when α becomes smaller as the interference contribution from far-off BSs carries more weight. Conversely, for large α the interference is dominated by only a few close-by BSs, thereby reducing the interference variance. For typical α in HetNets around $\alpha = 3.7$ [31], the variance is 0.74 when $S = 1$.
- With the same path loss law $\|\cdot\|^{-\alpha}$, the interference variance in the ad hoc network model is not defined [28], as interfering transmitters can be arbitrarily close to the receiver in this case. Although this result is due to the singularity of the path loss law and has no physical relevance, it follows that the interference variance in HetNets is tendentially smaller than in the ad hoc network model. This, in turn, suggests that interference-aware diversity combining will generally perform lower in HetNets. We shall discuss this further in Section V-B.

- The interference variance decays with the number of active Tx antennas S . This is because adding/activating more antennas while reducing the per-antenna transmit power by S smoothes out the channel fluctuations. This effect is also referred to as *channel-hardening* [32]. Hence, for large S we expect IA-MRC to perform similar to IB-MRC due to the higher interference correlation. In the limit $S \rightarrow \infty$, the interference variance becomes $\frac{1}{\alpha-1}$.

B. Normalized Interference Correlation across Antennas

In order to study the interference correlation across antennas, we first need the covariance of the normalized interference, conditioned on the serving tier ℓ and serving BS distance y . The covariance can be obtained as

$$\begin{aligned} \text{Cov}_{\ell,y}[I'_u, I'_v] &\stackrel{(a)}{=} \frac{y^{2\alpha_\ell}}{P_\ell^2} \sum_{k=1}^K \text{Cov}_{\ell,y}[I_{u,k}, I_{v,k}] \\ &\stackrel{(b)}{=} 2\pi y^{2\alpha_\ell} \sum_{k=1}^K \hat{P}_k^2 \lambda_k \frac{\mathbb{E}[\|\mathbf{h}_u(S_k)\|_F^2 \|\mathbf{h}_v(S_k)\|_F^2]}{S_k^2} \int_{d_k}^{\infty} r^{-2\alpha_k+1} dr \\ &\stackrel{(c)}{=} \pi \sum_{k=1}^K \frac{\lambda_k \hat{P}_k^{2/\alpha_k}}{\alpha_k - 1} y^{2/\alpha_k}, \end{aligned} \quad (10)$$

where (a) follows from $\text{Cov}[z_1 + c, z_2 + c] = \text{Cov}[z_1, z_2]$ and from the independence of the $I_{n,k}$ across k , (b) follows from Campbell's theorem [21] and from \mathbf{h}_n being independent across n , and (c) follows from Lemma 2. With (8) and (10), the conditional correlation coefficient becomes

$$\rho_{\ell,y} = \frac{\text{Cov}_{\ell,y}[I'_u, I'_v]}{\text{Var}_{\ell,y}[I'_n]} = \frac{\text{Cov}_{\ell,y}[I_{u,v}]}{\text{Var}_{\ell,y}[I_n]} \stackrel{S_k \equiv S}{=} \frac{S}{1 + S}. \quad (11)$$

The following observations can be made from (11):

- The correlation coefficient $\rho_{\ell,y}$ in (11) has the same form as in the ad hoc network model with Aloha, which was derived in [28, Lem. 5.13], though under the term *temporal* correlation coefficient. Temporal correlation and spatial correlation across antennas are mathematically the same, since in both cases fading varies while the interferer locations remain fixed.
- As expected, adding/activating more Tx antennas increases the interference correlation across Rx antennas, since the channel fluctuations then undergo an averaging effect. For $S = 1$ we have $\rho_{\ell,y} = 1/2$. In the limit $S \rightarrow \infty$, the interference correlation becomes maximal, i.e., $\rho_{\ell,y} = 1$. Similar to the above comment on interference variance for large S , IA-MRC is expected to have the same performance as IB-MRC in this regime.
- Interestingly, $\rho_{\ell,y}$ is independent from the tier with which the typical user associates and also from the distance to the serving BS. When the number of active Tx antennas is equal across tiers ($S_k \equiv S$), $\rho_{\ell,y}$ is unaffected by K , P_k , and λ_k . In contrast to the interference variance, the correlation is also independent from the path loss exponent in this case.

Remark 1 (Feasibility of Interference Estimation). *When the set of active antennas of interfering BSs changes in every slot*

τ , l_n varies unpredictably between every slot of the codeword. This is the case when $S_k < M_k$. Unfortunately, such rapid variations over τ are imperceptible to CSI estimation since the latter is usually designed to track channel-fading variations, which happen on a larger time scale. However, when full-rate OSTBCs are used ($r_k = 1$ for all k), l_n is identical across τ , since all $S_k = M_k$ antennas are always active. In that case, the receiver can obtain knowledge of l_n with acceptable complexity, e.g., by decoding also the cell-specific reference symbols of interfering BSs once within each frame.

IV. COVERAGE PROBABILITY ANALYSIS

We now study the downlink performance at the typical user for both IB-MRC and IA-MRC. As explained in Remark 1, IA-MRC is practical only for full-rate OSTBCs ($r_k = 1$ for all k). A common way for studying the performance of diversity-combining techniques is to analyze the post-combiner signal-to-interference-plus-noise ratio (SINR). The specific form of the SINR depends on the considered scheme and will be developed in Sections IV-A and IV-B.

Definition 1 (Coverage Probability P_c). *The coverage probability is defined as*

$$P_c \triangleq \mathbb{P}(\text{SINR} \geq T) \quad (12)$$

for a coding-/modulation-specific threshold $T > 0$.

The P_c can be interpreted as the SINR distribution at the typical user, or alternatively as the average fraction of users in the HetNet covered by an SINR no less than T .

A. MIMO Diversity with interference-blind MRC

An extremely useful property of OSTBCs is that the MIMO input-output relation, i.e., (4), can be reduced to parallel SISO channels [33]. At the typical user, having knowledge of \mathbf{H}_o , this is achieved by performing the linear combination $\sum_{n=1}^N \sum_{m=1}^{M_\ell} h_{o,nm}^* \mathbf{A}_{nm}^H \bar{\mathbf{y}} + h_{o,nm} \mathbf{B}_{nm}^T \bar{\mathbf{y}}^*$, where \mathbf{A}_{nm} and \mathbf{B}_{nm} are the $NT_\ell \times S_\ell$ dispersion matrices describing the OSTBC employed in the serving tier, see [34], [35] for further details. The resulting *equivalent channel model* allows treating the detection of each of the S_ℓ information symbols encoded in the current codeword separately. The corresponding SINR at the symbol decoder can then be expressed as

$$\text{SINR}_\ell(y) = \frac{P_\ell y^{-\alpha_\ell} \|\mathbf{H}_o\|_F^2 / S_\ell}{\sum_{k=1}^K \sum_{i \in \Phi_k^o} l_{i,\text{eqv}} + \sigma^2}, \quad (13)$$

where $l_{i,\text{eqv}}$ is the interference (power) from the i -th BS in the equivalent channel model. $l_{i,\text{eqv}}$ is statistically the same for all S_ℓ symbols. Thus, focusing on an arbitrary symbol, i.e., considering a single arbitrary column of \mathbf{A}_{nm} , \mathbf{B}_{nm} , say \mathbf{a}_{nm} , \mathbf{b}_{nm} , the interference $l_{i,\text{eqv}}$ is

$$l_{i,\text{eqv}} = \text{Var}_{\mathbf{c}_i} \left[\sum_{n=1}^N \sum_{m=1}^{M_\ell} \frac{h_{o,nm}^*}{\|\mathbf{H}_o\|_F} \mathbf{a}_{nm}^H \bar{\mathbf{i}}_i + \frac{h_{o,nm}}{\|\mathbf{H}_o\|_F} \mathbf{b}_{nm}^T \bar{\mathbf{i}}_i^* \right]. \quad (14)$$

Note that the receiver noise statistics remain unaffected by the linear combination [33], [35]. However, the distribution of $l_{i,\text{eqv}}$ is more complicated, particularly due to its dependence

on \mathbf{H}_o . This was already observed in [16] for a similar MIMO network model, where the authors also showed that ignoring this dependence and assuming $l_{i,\text{eqv}}$ to be Gamma distributed yields a valid approximation. We thus follow the same approach and assume $l_{i,\text{eqv}} \simeq P_k / \|\mathbf{x}_i\|^{\alpha_k} \|\mathbf{H}_i(S_k)\|_F^2 / S_k$ with $l_{i,\text{eqv}}$ being independent from \mathbf{H}_o . The following two facts support this approximation:

- It can be shown that the approximation is moment matching irrespective of the realization of \mathbf{H}_o , i.e., $\mathbb{E}_{\mathbf{H}_i}[l_{i,\text{eqv}}] = P_k / \|\mathbf{x}_i\|^{\alpha_k} \mathbb{E}_{\mathbf{H}_i}[\|\mathbf{H}_i(S_k)\|_F^2] / S_k = P_k / \|\mathbf{x}_i\|^{\alpha_k}$ in (14).
- Whenever $M_k = 1$, it follows from [29] that the above approximation becomes exact. In this case $l_{i,\text{eqv}}$ is also truly independent from \mathbf{H}_o .

Lemma 3 (Interference Laplace Transform). *Consider the interference field $l = \sum_{k=1}^K \sum_{i \in \Phi_k^o} P_k / \|\mathbf{x}_i\|^{\alpha_k} \|\mathbf{H}_i(S_k)\|_F^2 / S_k$. Its Laplace transform is given by*

$$\mathcal{L}_l(s) = e^{-\pi \sum_{k=1}^K \lambda_k d_k^2 \left({}_2F_1\left(-\frac{2}{\alpha_k}, S_k, 1 - \frac{2}{\alpha_k}; -\frac{s P_k}{S_k d_k^{\alpha_k}}\right) - 1 \right)}. \quad (15)$$

Proof: We write

$$\begin{aligned} \mathbb{E} \left[\exp \left(-s \sum_{k=1}^K \sum_{i \in \Phi_k^o} \frac{P_k}{S_k \|\mathbf{x}_i\|^{\alpha_k}} \|\mathbf{H}_i(S_k)\|_F^2 \right) \right] \\ &\stackrel{(a)}{=} \prod_{k=1}^K \mathbb{E} \left[\prod_{i \in \Phi_k^o} \mathcal{L}_{\|\mathbf{H}_i(S_k)\|_F^2} \left(\frac{s P_k}{S_k \|\mathbf{x}_i\|^{\alpha_k}} \right) \right] \\ &\stackrel{(b)}{=} \prod_{k=1}^K \mathbb{E} \left[\prod_{i \in \Phi_k^o} \left(1 + \frac{s P_k}{S_k \|\mathbf{x}_i\|^{\alpha_k}} \right)^{-S_k} \right] \\ &\stackrel{(c)}{=} \exp \left\{ -\pi \sum_{k=1}^K \lambda_k \int_{d_k}^{\infty} 2r \left(1 - \frac{1}{\left(1 + \frac{s P_k}{S_k r^{\alpha_k}} \right)^{S_k}} \right) dr \right\}, \end{aligned} \quad (16)$$

where (a) follows from the independence of the Φ_k^o across k and from the independence of the $\|\mathbf{H}_i(S_k)\|_F^2$ across i , (b) follows from the Laplace transform of the Erlang distributed $\|\mathbf{H}_i(S_k)\|_F^2$, and (c) follows from the probability generating functional (PGFL) for PPPs, see [21]. ■

We now have the tools required to characterize the coverage probability for IB-MRC.

Theorem 1 (P_c for Interference-Blind MRC). *The coverage probability P_c^{IB} for IB-MRC in the described setting is given by (17) at the top of the next page, where $\overline{\text{SINR}}_\ell(y) \triangleq P_\ell y^{-\alpha_\ell} / \sigma^2$ and $\hat{S}_k \triangleq S_k / S_\ell$.*

Proof: See Appendix A. ■

The Gaussian hypergeometric function ${}_2F_1(\cdot, \cdot, \cdot; \cdot)$ can be expressed through elementary functions [36] for certain α_k . For instance, ${}_2F_1(1, -\frac{1}{2}, \frac{1}{2}; -u) = 1 + \sqrt{u} \arctan \sqrt{u}$ when $\alpha_k = 4$. For general $\alpha_k > 2$, (17) can be easily evaluated using standard numerical software programs.

The differentiation d^m/ds^m in (17) can be calculated using Faà di Bruno's formula for higher-order derivatives of composite functions [36], i.e., functions consisting of an inner and an outer function. While the outer function of the integrand is

$$P_c^{\text{IB}} = 2\pi \sum_{\ell=1}^K \sum_{m=0}^{NM_\ell-1} \frac{(-1)^m \lambda_\ell}{m!} \int_0^\infty y \frac{d^m}{ds^m} \left[\exp \left(-\frac{s S_\ell T}{\text{SNR}_\ell(y)} - \pi \sum_{k=1}^K \lambda_k \hat{P}_k^{2/\alpha_k} y^{2/\hat{\alpha}_k} {}_2F_1 \left(-\frac{2}{\alpha_k}, S_k, 1 - \frac{2}{\alpha_k}; -\frac{sT}{\hat{S}_k} \right) \right) \right] dy \quad (17)$$

$$P_c^{\text{IA}} = 2\pi \sum_{\ell=1}^K \sum_{m=0}^{M_\ell-1} \frac{(-1)^{m+M_\ell} \lambda_\ell}{m! \Gamma(M_\ell)} \int_0^\infty \int_0^\infty y z^{-1} \frac{d^m}{ds^m} \frac{d^{M_\ell}}{dt^{M_\ell}} \left[\exp \left(-\frac{M_\ell}{\text{SNR}_\ell(y)} (s(T-z)^+ + tz) \right) \right. \\ \left. \times \exp \left(-\pi \sum_{k=1}^K \lambda_k \hat{P}_k^{2/\alpha_k} y^{2/\hat{\alpha}_k} \left[1 + \Psi \left(\frac{s(T-z)^+}{\hat{M}_k}, \frac{tz}{\hat{M}_k}, M_k, \alpha_k \right) \right] \right) \right] dy dz, \quad 1 \leq M_k \leq 2, N=2 \quad (26)$$

simple due to the exp-term, the inner function, more specifically the ${}_2F_1 \left(-2/\alpha_k, S_k, 1 - 2/\alpha_k; -sT/\hat{S}_k \right)$ expression, is more involved. With [36], its derivative is obtained as

$$\frac{d^m}{ds^m} \left[{}_2F_1 \left(-\frac{2}{\alpha_k}, S_k, 1 - \frac{2}{\alpha_k}; -\frac{sT}{\hat{S}_k} \right) \right]_{s=1} \\ = \left(-\frac{T}{\hat{S}_k} \right)^m \frac{-2/\alpha_k \Gamma(S_k + m)}{(m - 2/\alpha_k) \Gamma(S_k)} \\ \times {}_2F_1 \left(-\frac{2}{\alpha_k} + m, S_k + m, 1 - \frac{2}{\alpha_k} + m; -\frac{T}{\hat{S}_k} \right). \quad (18)$$

In dense deployments the performance is typically limited by interference rather than noise [37], which yields $\sigma^2 = 0 \Leftrightarrow \text{SNR}_\ell(y) = 0$ for all ℓ, y . In addition, the path loss exponent does not vary significantly across tiers in practice with typical values around $\alpha_k \approx 3.7$ [31]. When in addition the number of Tx antennas is also equal across tiers, the following corollary applies.

Corollary 1 (Special Case). *In the absence of receiver noise ($\sigma^2 = 0$) and with equal path loss exponents ($\alpha_k \equiv \alpha$) and number of Tx antennas ($M_k \equiv M$, $S_k \equiv S$), P_c^{IB} simplifies to*

$$P_c^{\text{IB}} = \sum_{m=0}^{NM-1} \frac{(-1)^m}{m!} \frac{d^m}{ds^m} \left[\frac{1}{{}_2F_1 \left(-\frac{2}{\alpha}, S, 1 - \frac{2}{\alpha}; -sT \right)} \right]_{s=1} \quad (19)$$

The coverage probability in (19) neither depends on the BS densities λ_k and powers P_k , nor on the number of tiers K , which is consistent with the literature, see for instance [24]. Note that the first term $m = 0$ in (19) corresponds to the coverage probability for the SISO case [23].

B. MIMO Diversity with interference-aware MRC

We now assume $M_k \leq 2$ for all K tiers. This ensures that the receiver can estimate the interference with acceptable complexity once within the current block/frame, see Remark 1. In this case we have $S_k = M_k$. When $M_k \leq 2$, tier k uses either Alamouti space-time coding ($M_k = 2$) or no space-time coding ($M_k = 1$). In both cases, the interference power remains constant in each codeword slot. Its value at the n -th antenna is given by (7). We assume that the receiver knows the current per-antenna interference-plus-noise power $\mathbf{l}_n + \sigma^2$ at each antenna, in addition to the channel gains of the desired link. Interference is treated as white noise.

In IA-MRC, the phase-corrected and channel-weighted received signals are additionally scaled by the interference-plus-noise power experienced at each antenna, thereby following

the original MRC approach from [10]. The receiver hence performs the linear combination

$$\sum_{n=1}^N \sum_{m=1}^{M_\ell} \frac{h_{o,nm}^*}{\mathbf{l}_n + \sigma^2} \mathbf{A}_{nm}^H \bar{\mathbf{y}} + \frac{h_{o,nm}}{\mathbf{l}_n + \sigma^2} \mathbf{B}_{nm}^T \bar{\mathbf{y}}^*, \quad (20)$$

yielding the equivalent channel model for IA-MRC. Similar to Section IV-A, we focus again on an arbitrary symbol and therefore consider an arbitrary column \mathbf{a}_{nm} , \mathbf{b}_{nm} of \mathbf{A}_{nm} , \mathbf{B}_{nm} . The SINR for IA-MRC can then be expressed as

$$\text{SINR}_\ell(y) = \frac{\frac{P_\ell}{M_\ell y^{\alpha_\ell}} \left(\sum_{n=1}^N \frac{\|\mathbf{h}_{o,n}\|_F^2}{\mathbf{l}_n + \sigma^2} \right)^2}{\sum_{k=1}^K \sum_{i \in \Phi_k^o} \mathbf{l}_{i,\text{eqv}} + \sum_{n=1}^N \frac{\|\mathbf{h}_{o,n}\|_F^2 \sigma^2}{\mathbf{l}_n + \sigma^2}}, \quad (21)$$

where now $\mathbf{l}_{i,\text{eqv}}$ is

$$\mathbf{l}_{i,\text{eqv}} = \text{Var}_{\mathbf{c}_i} \left[\sum_{n=1}^N \sum_{m=1}^{M_\ell} \frac{h_{o,nm}^*}{\mathbf{l}_n + \sigma^2} \mathbf{a}_{nm}^H \bar{\mathbf{i}}_i + \frac{h_{o,nm}}{\mathbf{l}_n + \sigma^2} \mathbf{b}_{nm}^T \bar{\mathbf{i}}_i^* \right] \quad (22)$$

With the orthogonality property of \mathbf{A}_{nm} , \mathbf{B}_{nm} , see for instance [29], (22) can be computed as

$$\mathbf{l}_{i,\text{eqv}} = \frac{P_k}{M_k \|\mathbf{x}_i\|^{\alpha_k}} \sum_{n=1}^N \|\mathbf{h}_{o,n}\|_F^2 \frac{\|\mathbf{h}_{i,n}\|_F^2}{\mathbf{l}_n + \sigma^2} + \frac{Z_{i,n}}{\mathbf{l}_n + \sigma^2}, \quad (23)$$

where $Z_{i,n}$ describes the part resulting from the non-zero off-diagonal elements of the covariance matrix $\mathbb{E}_{\mathbf{c}_i} [\bar{\mathbf{i}}_i \bar{\mathbf{i}}_i^H]$. $Z_{i,n}$ depends on the relative channel phases of \mathbf{H}_i . Since the $h_{i,nm}$ are $\mathcal{CN}(0, 1)$ distributed, it can be shown that $\mathbb{E}_{\mathbf{H}_i} [Z_{i,n}] = 0$ irrespective of \mathbf{H}_o , thus the effect of $Z_{i,n}$ vanishes in the long run. To obtain a more tractable SINR expression, we hence ignore $Z_{i,n}$. After some simple algebraic manipulations, the simplified SINR from (21) becomes

$$\text{SINR}_\ell(y) = \frac{P_\ell}{M_\ell y^{\alpha_\ell}} \sum_{n=1}^N \frac{\|\mathbf{h}_{o,n}\|_F^2}{\mathbf{l}_n + \sigma^2}. \quad (24)$$

Remark 2 (SINR-Approximation). *It follows by Jensen's Inequality [38] that*

$$\mathbb{E}_{\mathbf{H}_1, \mathbf{H}_2, \dots} [\text{SINR}_\ell(y)] \geq \frac{P_\ell}{M_\ell y^{\alpha_\ell}} \sum_{n=1}^N \frac{\|\mathbf{h}_{o,n}\|_F^2}{\mathbf{l}_n + \sigma^2}, \quad (25)$$

where $\text{SINR}_\ell(y)$ on the left-hand side corresponds to the exact SINR from (21). Hence, the simplified SINR from (24) provides a lower bound to the phase-averaged exact SINR. The resulting error when (24) is used to approximate the exact SINR is barely noticeable, as confirmed by simulations in Section V.

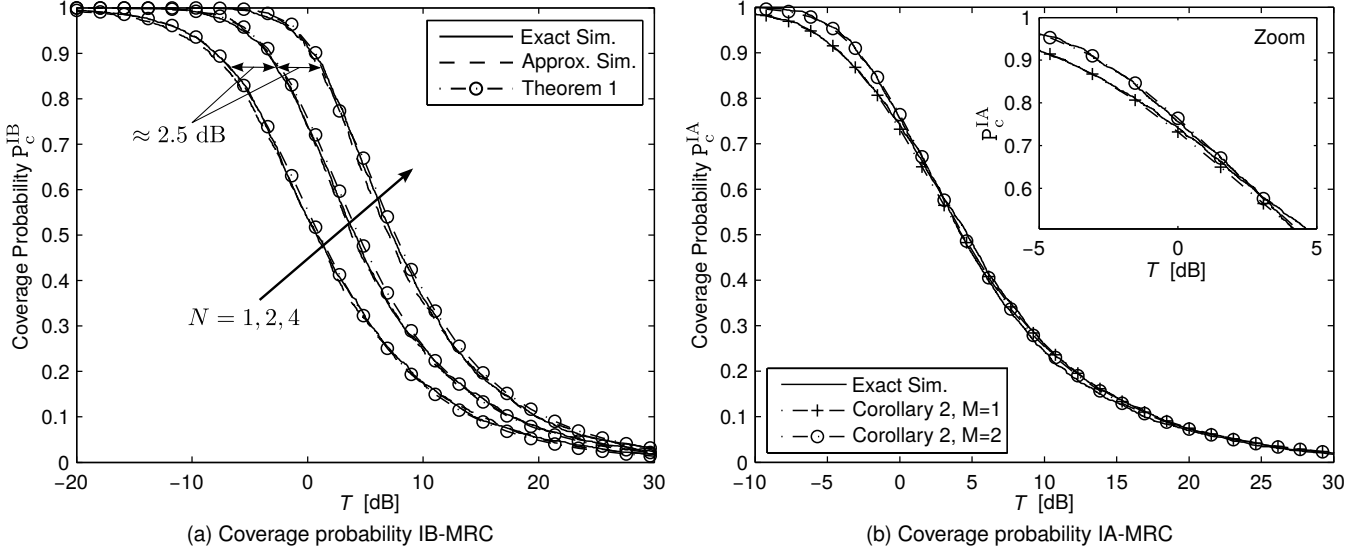


Fig. 2. (a) Coverage probability P_c^{IB} for different N . Receiver noise is $\sigma^2 = -104$ dBm. (b) Coverage probability P_c^{IA} for $\alpha = 3.7$, $\sigma^2 = 0$, and $M = 1, 2$.

Although the $\mathbf{h}_{i,n}$ in (24) are mutually independent, the l_n are correlated across Rx antennas due to the common locations of interfering BSs. More specifically, the expression in (24) is a sum of correlated random variables exhibiting a complicated correlation structure. This renders the computation of the coverage probability for IA-MRC for general N challenging. In practical systems, however, the number of antennas mounted on mobile devices is limited due to space/complexity limitations, thereby often not exceeding $N = 2$. This case is addressed next.

Theorem 2 (P_c for Interference-Aware MRC). *The coverage probability P_c^{IA} for IB-MRC in the described setting with $M_k \leq 2$ is given by (26) at the top of the previous page, where $\Psi(\cdot, \cdot, \cdot, \cdot)$ is given by (48) and $\hat{M}_k \triangleq M_k/M_\ell$.*

Proof: See Appendix B. ■

The function $\Psi(\cdot, \cdot, \cdot, \cdot)$ in (26) can be given in terms of Gaussian hypergeometric functions ${}_2F_1(\cdot, \cdot, \cdot; \cdot)$, which can be further simplified in some cases, see comment after Theorem 1 in Section IV-A. We shall exploit this fact in Section V-B.

Compared to P_c^{IB} in (17), P_c^{IA} is more involved due to the mathematical form of (24), which translates into the convolution-type integral over z . Nevertheless, the expression in (26) can be evaluated with acceptable complexity using semi-analytical tools, see for instance [19]. Besides, (26) covers the general case and the expression can be further simplified in certain specific cases as discussed next. The counterpart to Corollary 1 is given next.

Corollary 2 (Special Case). *In the absence of receiver noise ($\sigma^2 = 0$), and with equal path loss exponents ($\alpha_k \equiv \alpha$) and number of Tx antennas ($M_k \equiv M \leq 2$), P_c^{IA} reduces to*

$$P_c^{\text{IA}} = \sum_{m=0}^{M-1} \frac{(-1)^{m+M}}{m! \Gamma(M)} \int_0^\infty z^{-1}$$

$$\times \frac{d^m}{ds^m} \frac{d^M}{dt^M} \left[\frac{1}{1 + \Psi(s(T-z)^+, tz, M, \alpha)} \right]_{s=1} dz. \quad (27)$$

The expression in (27) is less complicated than (26). When the SINR threshold T is not large, the $\Psi(s(T-z)^+, tz, M, \alpha)$ term can be further simplified as shown next.

Corollary 3 (Small- T Approximation). *For small T the following approximation becomes tight*

$$1 + \Psi\left(\frac{s(T-z)^+}{\hat{M}_k}, \frac{tz}{\hat{M}_k}, M_k, \alpha_k\right) \simeq {}_2F_1\left(-\frac{2}{\alpha_k}, M_k, 1 - \frac{2}{\alpha_k}; -\frac{s(T-z)^+ + tz}{\hat{M}_k}\right). \quad (28)$$

The right-hand side of (28) may be easier to evaluate than the original expression since the Gaussian hypergeometric function is available in most numerical software programs. Moreover, its higher-order derivatives with respect to both s and t appearing in (26) can be evaluated fairly easily following the same procedure as in (18) for differentiating composite functions.

V. NUMERICAL EXAMPLES AND DESIGN INSIGHTS

In this section, we leverage the theoretical results developed in Sections III and IV to understand the system behavior of MIMO diversity in HetNets through numerical examples. Besides, the theoretic expressions including the approximations involved (see Sections IV-A and IV-B), are verified by numerical simulations. Unless stated otherwise, we assume a three-tier HetNet ($K = 3$) with the tier-specific system parameters given in Table II, see [31]. The dispersion matrices \mathbf{A}_{nm} , \mathbf{B}_{nm} are obtained using [29, Sec. 2.2.3].

A. Multi-Tier & MIMO: IB-MRC vs IA-MRC

We first focus on IB-MRC and consider a typical HetNet scenario with the parameters shown in Table II. The

TABLE II
SYSTEM PARAMETERS USED FOR NUMERICAL EXAMPLES

Parameter	Tier 1	Tier 2	Tier 3
BS density λ_k	4 BS/km ²	16 BS/km ²	40 BS/km ²
BS power P_k	46 dBm	30 dBm	24 dBm
BS Tx antennas M_k	4	2 (Alamouti)	1 (no OSTBC)
Path loss exponent α_k	3.76	3.67	3.5

(4, 4, 3/4)-OSTBC from [30, 7.4.10] is chosen for tier one. Fig. 2a shows the coverage probability P_c^{IB} versus the SINR threshold T for IB-MRC and different number of Rx antennas N . It can be seen that the theoretical expressions perfectly match the simulation results. Furthermore, the simulation results for the interference Gamma approximation explained in Section IV-A (Approx. Sim.) and for the exact case (Exact Sim.) are hardly distinguishable, which is consistent with [16]. As expected, increasing N improves P_c^{IB} since the typical user enjoys a larger array gain. For operational points of practical relevance, i.e. around 80% of covered users, the horizontal gap between the curves in Fig. 2a is roughly 2.5 dB. For IA-MRC, doubling the number of Rx antennas yields a gain of roughly 3.6 dB (verified by simulations for $N > 2$).

Figure 2b shows the coverage probability P_c^{IA} for IA-MRC. Here, we consider the interference-limited case ($\sigma^2 = 0$) with homogeneous path loss exponents ($\alpha_k = 3.7$) and the same number of Tx antennas ($M_k \equiv M$). Again, simulation results and theoretic expressions (Corollary 2) are fairly close over the entire range of T , thereby justifying the approximation made in Section IV-B, see Remark 2. It can be further observed that, for IA-MRC, adding a second Tx antenna and performing Alamouti space-time coding slightly improves the performance only at low T . This gain, about 4% in the practically relevant regime, is comparable to the gain due to frequency-diversity based resource allocation in SISO HetNets [39]. The same behavior (gain around 4%) was observed also for IB-MRC. This rather minor improvement from Tx diversity is well-known in the literature [37] and is reconfirmed and quantified for MIMO HetNets with MRC here.

Next, we compare the performance of IB-MRC and IA-MRC for the same scenario, i.e., $\sigma^2 = 0$, $\alpha_k = 3.7$ and ($M_k \equiv M$). In Fig. 3, the relative coverage probability gain of IA-MRC over IB-MRC is shown for $M = 1, 2$ Tx antennas. This gain, however, is somewhat small ($< 2\%$ in this example). In fact, IA-MRC becomes even less favorable when adding more Tx antennas. This is due to the fact that adding more antennas effectively smoothes out the fading on the interfering channels, so that the interference becomes more and more similar across Rx antennas. This effect was already predicted in Section III, where the second-order statistics of the interference were analyzed. Thus, with almost equal interference at all the branches, the performance of IB-MRC and IA-MRC become similar due to lack of sufficient (interference) diversity. In conclusion, the additional though not overwhelming complexity of IA-MRC must hence be traded-off against an insignificant performance improvement relative to IB-MRC; with Tx diversity activated, IB-MRC might then

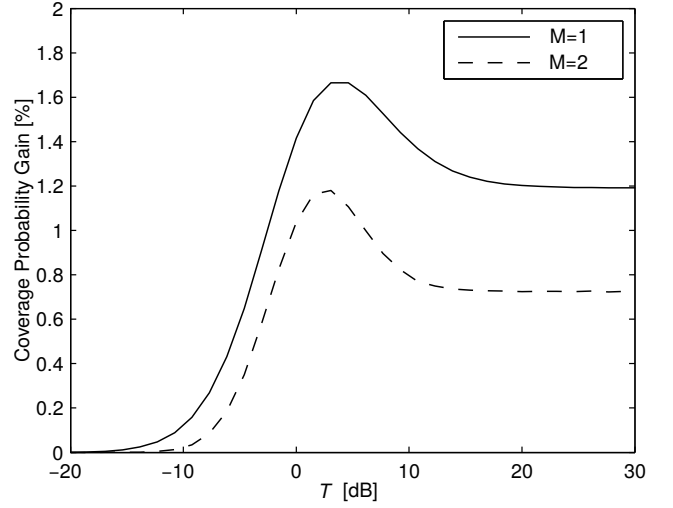


Fig. 3. Relative coverage probability gain of IA-MRC over IB-MRC for $\alpha = 3.7$, $\sigma^2 = 0$, and $M = 1, 2$.

be the better choice.

B. Multi-Tier & SIMO: Gain of MRC over SISO

From an information-theoretic viewpoint, Rx diversity with MRC is more appealing than Tx diversity with space-time coding as the latter incurs a power penalty [37]. But the potential gains of Rx diversity with MRC in HetNets, however, are not yet well-understood due to their dependence on many system parameters. While in Section V-A the relative performance of IB-MRC and IA-MRC was studied, we now focus on the gains provided solely by MRC Rx diversity ($M_k = 1$) over SISO transmission. For that, we consider again the interference-limited regime ($\sigma^2 = 0$) with the equal path loss exponents across tiers ($\alpha_k \equiv \alpha$) and $N = 2$. In this case, we obtain the simple expressions

$$P_c^{\text{IB}} = \frac{1}{2F_1\left(-\frac{2}{\alpha}, 1, 1 - \frac{2}{\alpha}; -T\right)} + \underbrace{\frac{\frac{d}{ds} [2F_1\left(-\frac{2}{\alpha}, 1, 1 - \frac{2}{\alpha}; -sT\right)]_{s=1}}{2F_1\left(-\frac{2}{\alpha}, 1, 1 - \frac{2}{\alpha}; -T\right)^2}}_{\triangleq G^{\text{IB}}(\alpha, T)} \quad (29)$$

for IB-MRC and

$$P_c^{\text{IA}} = \frac{1}{2F_1\left(-\frac{2}{\alpha}, 1, 1 - \frac{2}{\alpha}; -T\right)} + \underbrace{\int_0^T \frac{\frac{d}{dz} [\mathcal{A}(T-z, tz, \alpha)]_{t=1}}{z \mathcal{A}(T-z, z, \alpha)^2} dz}_{\triangleq G^{\text{IA}}(\alpha, T)} \quad (30)$$

for IA-MRC, where $\mathcal{A}(\cdot, \cdot, \cdot) \triangleq 1 + \Psi(\cdot, \cdot, 1, \cdot)$ is

$$\mathcal{A}(a_1, a_2, q) = \frac{a_1}{a_1 - a_2} {}_2F_1\left(-\frac{2}{q}, 1, 1 - \frac{2}{q}; -a_1\right) - \frac{a_2}{a_1 - a_2} {}_2F_1\left(-\frac{2}{q}, 1, 1 - \frac{2}{q}; -a_2\right). \quad (31)$$

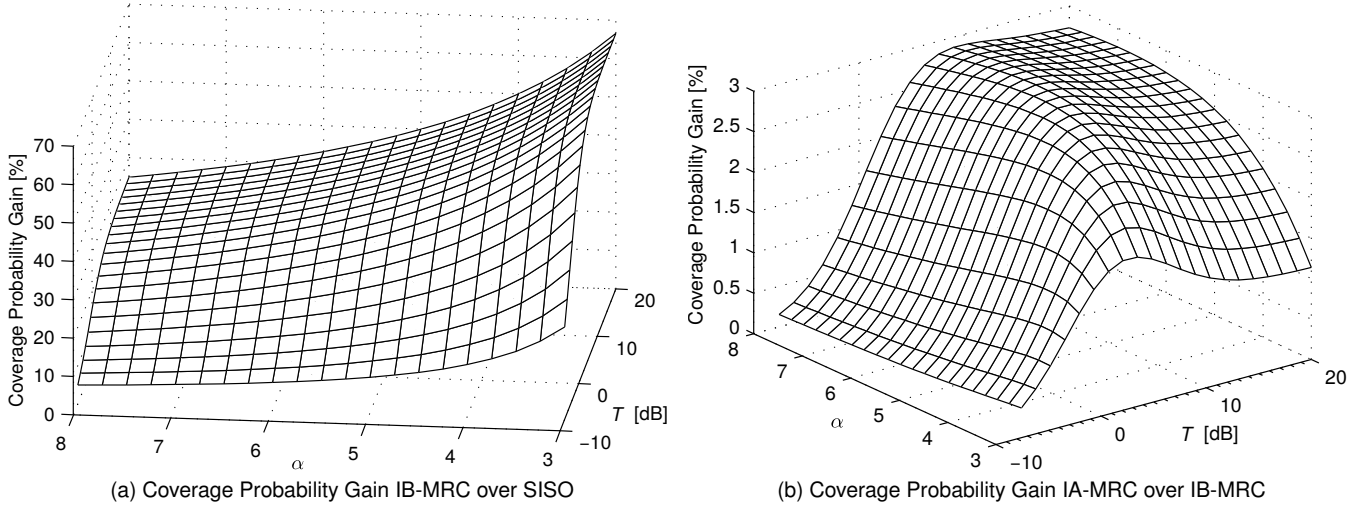


Fig. 4. Parameters: $M = 1$, $N = 2$, $\alpha_k \equiv \alpha$, and $\sigma^2 = 0$. (a) Gain of IB-MRC over SISO. (b) Gain of IA-MRC over IB-MRC.

Remark 3. The first term in (29) and (30) corresponds to the SISO coverage probability [23]

$$p_c^{\text{SISO}} = \frac{1}{{}_2F_1\left(-\frac{2}{\alpha}, 1, 1 - \frac{2}{\alpha}; -T\right)}. \quad (32)$$

This, in turn, means that $G^{\text{IB}}(\alpha, T)$ in (29) and $G^{\text{IA}}(\alpha, T)$ in (30) fully characterize the coverage probability gain of dual-antenna IB-MRC and IA-MRC, respectively, over SISO in HetNets.

The derivative inside $G^{\text{IB}}(\alpha, T)$ and $G^{\text{IA}}(\alpha, T)$ can be computed using (18). For IA-MRC, $G^{\text{IA}}(\alpha, T)$ can be expressed by the closed-form integral in (33) at the top of the next page.

As a consequence of Remark 3, we can identify $G^{\text{IB}}(\alpha, T)$ and $G^{\text{IA}}(\alpha, T)$ as the characteristic terms for analyzing the performance of dual-branch MRC relative to SISO transmission. For instance, the relative coverage probability improvement of dual-branch IB-MRC over SISO transmission can be written as $(p_c^{\text{IB}} - p_c^{\text{SISO}})/p_c^{\text{SISO}} = G^{\text{IB}}(\alpha, T) {}_2F_1(-2/\alpha, 1, 1 - 2/\alpha; -T)$.

Figure 4a shows the relative coverage probability increase of IB-MRC over SISO transmission versus α and T . The improvement monotonically decreases with α and monotonically increases with T . Interestingly, the improvement converges to a non-zero constant as T increases, although in the interference-free case the improvement (measured in 1-outage probability) is known to tend to zero [37, 7.2.4]. For typical operating points ($3 < \alpha < 5$ and $T > -6$ dB), the improvement obtained by IB-MRC is between 12%–66%. Fig. 4b illustrates the additional improvement over SISO when switching from IB-MRC to IA-MRC. In line with Fig. 3, IB-MRC already harvests most of the gains over SISO transmission as the additional improvement of IA-MRC does not exceed 3%. Nevertheless, the largest additional improvement for realistic path loss exponents around $\alpha = 4$ lies entirely in the practical regime $-5 < T < 10$.

C. Effect of Spatial Interference Correlation

As already explained in Section I and III, spatial interference correlation influences the performance of IA-MRC. Mathe-

matically, this can be seen by noting that the post-combiner SINR in (24) exhibits a complicated correlation structure, which was addressed by the theoretic machinery developed in Section IV-B. To circumvent this rather involved mathematical effort, two simpler correlation models are typically used in the literature: 1) no-correlation model, and 2) full-correlation model. Using the results from Section IV-B, the validity of these models will be discussed in the following.

1) *No-Correlation Model:* A commonly made assumption to maintain analytical tractability is to assume that the l_n in (24) are uncorrelated, i.e., the locations of interfering BSs in l_n originate from separate independent point processes for each antenna n . Under this assumption, we obtain the following coverage probability $p_{c,\text{NC}}^{\text{IA}}$ for the no-correlation model.

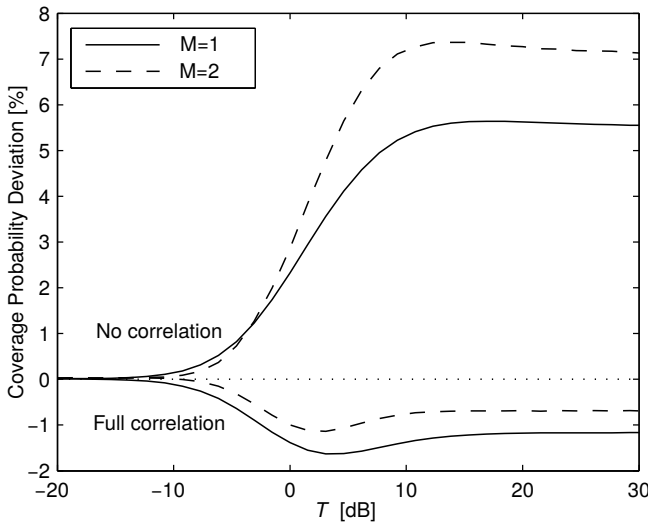
Proposition 1 (Coverage Probability $p_{c,\text{NC}}^{\text{IA}}$). The coverage probability $p_{c,\text{NC}}^{\text{IA}}$ for 2-antenna IA-MRC in the no-correlation model is given by (26) with $1 + \Psi(\cdot, \cdot, \cdot, \cdot)$ replaced by

$${}_2F_1\left(-\frac{2}{\alpha_k}, M_k, 1 - \frac{2}{\alpha_k}; -\frac{s}{M_k} (T - z)^+\right) + {}_2F_1\left(-\frac{2}{\alpha_k}, M_k, 1 - \frac{2}{\alpha_k}; -\frac{t}{M_k} z\right) - 1. \quad (34)$$

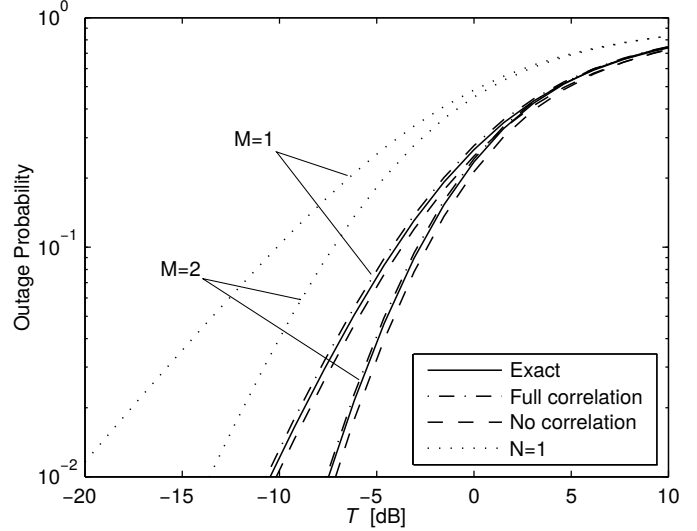
Proof: See Appendix C. ■

By comparing the mathematical form of the expression in (34) with $1 + \Psi(\cdot, \cdot, \cdot, \cdot)$ in (26), the influence of spatial interference correlation becomes apparent: in (34) the sum of the $(T - z)^+$ and z related parts results in a factorization of the PDFs $f_{\text{SINR}_1}(T - z)$ and $f_{\text{SINR}_2}(z)$ in the integral over z , which corresponds to the well-known convolution-type integral for sums of independent random variables [38]. A closer look at $1 + \Psi(\cdot, \cdot, \cdot, \cdot)$ shows that no such factorization of the joint PDF of SINR_1 and SINR_2 can be made due to their correlation across Rx antennas.

2) *Full-Correlation Model:* Another frequently used technique in the literature to simplify the analysis is to assume that the l_n are fully correlated, i.e., the fading gains $\mathbf{h}_{i,n}$ yield the same realization across n for all $i \in \Phi^o$. Under



(a) Comparison with No- and Full-Correlation Model for IA-MRC



(b) Asymptotic Outage Probability for IA-MRC

Fig. 5. (a) Relative coverage probability deviation of no-correlation and full-correlation model for $M_k \equiv M = 1, 2$. (b) Outage probability comparison between exact correlation, no-correlation and full-correlation models for different $M_k \equiv M = 1, 2$. Results for single-Rx-antenna case ($N = 1$) are also shown for reference. Parameters are $\sigma^2 = 0$ and $\alpha_k \equiv \alpha = 3.7$.

$$G^{\text{IA}}(\alpha, T) = \int_0^T \frac{2T-4z}{z+1} - \frac{[(T(2+\alpha) - z(4+\alpha)) {}_2F_1(1, -\frac{2}{\alpha}, 1 - \frac{2}{\alpha}; -z) + \alpha(z-T) {}_2F_1(1, -\frac{2}{\alpha}, 1 - \frac{2}{\alpha}; -T+z)]}{\alpha [z {}_2F_1(1, -\frac{2}{\alpha}, 1 - \frac{2}{\alpha}; -z) + (-T+z) {}_2F_1(1, -\frac{2}{\alpha}, 1 - \frac{2}{\alpha}; -T+z)]^2} dz \quad (33)$$

$$P_c^{\text{SC}} = 2\pi \sum_{\ell=1}^K \sum_{n=1}^N (-1)^{n+1} \binom{N}{n} \lambda_\ell \int_0^\infty y \exp\left(-\frac{nT}{\text{SNR}_\ell(y)} - \pi \sum_{k=1}^K \lambda_k \hat{P}_k^{2/\alpha_k} y^{2/\alpha_k} {}_2F_1\left(-\frac{2}{\alpha_k}, n, 1 - \frac{2}{\alpha_k}; -T\right)\right) dy \quad (35)$$

this assumption, the corresponding coverage probability $P_{c,\text{FC}}^{\text{IA}}$ for the full-correlation model can be derived for an arbitrary N as shown next.

Proposition 2 (Coverage Probability $P_{c,\text{FC}}^{\text{IA}}$). *The coverage probability $P_{c,\text{FC}}^{\text{IA}}$ for N -antenna IA-MRC in the full-correlation model is the same as for IB-MRC, see (17) in Theorem 1.*

Proof: Since $\mathbf{h}_{i,u} \equiv \mathbf{h}_{i,v}$ for all $u, v \in [1, \dots, N]$ and $i \in \Phi^o$, it follows that $\mathbf{l}_u \equiv \mathbf{l}_v$ for all $u, v \in [1, \dots, N]$. Then, the SINR expression for IA-MRC in (24) collapses to the SINR expression in (13) for IB-MRC. ■

Figure 5a shows the coverage probability deviation for the two simpler correlation models for $M = 1$ and $M = 2$. The deviation is defined as $P_{c,\text{NC}}^{\text{IA}}/P_c^{\text{IA}} - 1$ ($P_{c,\text{FC}}^{\text{IA}}/P_c^{\text{IA}} - 1$) for the respective correlation models. First, it can be seen that both models reflect the true performance at small T . For $T > 0$ dB, the no-correlation model yields a significantly optimistic performance prediction (P_c gap is 3%–8%), depending on the number of Tx antennas. In contrast, the full-correlation model slightly underestimates the true performance (P_c gap $< 2\%$). In line with our intuition, adding a second Tx antenna increases the deviation in the no-correlation model due to the smaller interference variance and larger interference correlation across Rx antennas, see Section III. Consequently, the deviation decreases in the full-correlation model in this case. Varying the path loss exponent has the same effect as observed in

[20] for single-tier single-Tx-antenna cellular networks and is therefore not shown here. The smaller deviation of the full-correlation model was already reported in [19] for ad hoc networks and is reconfirmed in this work for HetNets. Fig. 5b illustrates the outage probability ($1 - P_c$) for the exact, no-correlation and full-correlation models for $M = 1$ and $M = 2$. It can be seen that the simpler correlation models preserve the true diversity order for dual-antenna IA-MRC. Interestingly, the diversity order due to IA-MRC (which is equal to N) remains unaffected by the interference correlation across antennas. This is in contrast to ad hoc networks, where, unlike in HetNets, interfering transmitters may be significantly closer to the receiver than the desired transmitter due to lack of medium access coordination [19]. As expected, the diversity order for $M = 2$ and $N = 2$ IA-MRC is $NM = 4$.

In conclusion, the full-correlation model offers a tight approximation to the performance of IA-MRC in HetNets, particularly when BSs employ multiple Tx antennas. This result is congruent with the prior observation that the performance gap between IA-MRC and IB-MRC is not significant and further decreases with the number of Tx antennas.

D. Comparison with Selection Combining

Complexity constraints may sometimes prohibit the use of MRC, thereby allowing only for combining schemes with lower complexity. Importantly, while hardware requirements of

combining schemes are independent from the communication environment, their performance obviously is not. To properly balance complexity-performance trade-offs, it is hence important to compare the performance of MRC to other combining schemes within a realistic model. We do this next for the example of SC, which is a widespread scheme with lower complexity compared to MRC. A similar comparison can be found in [19] for ad hoc networks and [20] for single-tier networks. We next focus on case $M_k \equiv M = 1$ and defer an extension to $M_k > 1$ to possible future work. The following result is a generalization of [26] and gives the coverage probability for SC, which we denote by P_c^{SC} .

Theorem 3 (Coverage Probability P_c^{SC}). *The coverage probability P_c^{SC} for SC in the described setting with $M_k \equiv M = 1$ is given by (35) at the top of the previous page.*

Proof: By [26, Eq. (8)], we can express P_c^{SC} as

$$P_c^{\text{SC}} = \sum_{n=1}^N (-1)^{n+1} \binom{N}{n} P_n(T), \quad (36)$$

where $P_n(T) \triangleq \mathbb{P}(\text{SINR}_1 > T, \dots, \text{SINR}_n > T)$ is the *joint success probability*, i.e., the probability of the SINR being greater than T at n antennas simultaneously. Invoking Lemma 1 and following the same line of thoughts as in [27, Appendix A], the conditional $P_{n,\ell}(T, y)$ (conditioned on tier ℓ and serving BS distance y) can be written as

$$\begin{aligned} P_{n,\ell}(T, y) &\stackrel{(a)}{=} \mathbb{E}_{\Phi^o} \left[\prod_{q=1}^n \mathbb{P} \left(|h_{o,q}|^2 > \frac{T y^\alpha}{P_\ell} (I_q + \sigma^2) | \Phi^o \right) \right] \\ &\stackrel{(b)}{=} \exp \left(-\frac{nT}{\overline{\text{SNR}}_\ell(y)} \right) \prod_{k=1}^K \mathbb{E} \left[\prod_{i \in \Phi_k^o} \left(1 + T \frac{y^{\alpha_\ell} \hat{P}_k}{\|x_i\|^{\alpha_k}} \right)^{-n} \right], \end{aligned} \quad (37)$$

where (a) follows from the independence of the $h_{o,q}$ across Rx antennas and (b) follows from the independence of the interfering channel gains $h_{i,q}$ and from the independence of the Φ_k^o across k . Applying Lemma 3 to (37) and de-conditioning on ℓ and y yields the result. ■

When receiver noise can be ignored and the path loss exponent does not vary significantly across tiers, (35) can be further simplified.

Corollary 4 (Special Case). *In the absence of receiver noise ($\sigma^2 = 0$) and with equal path loss exponent ($\alpha_k \equiv \alpha$), P_c^{SC} simplifies to*

$$P_c^{\text{SC}} = \sum_{n=1}^N \frac{(-1)^{n+1} \binom{N}{n}}{{}_2F_1\left(-\frac{2}{\alpha}, n, 1 - \frac{2}{\alpha}; -T\right)}. \quad (38)$$

Remark 4 (Comment on Corollary 4). *This corollary coincides with the result in [25, Corollary 2] for SC over multiple resource blocks without receiver noise in single-tier networks. Thus, Corollary 4, and especially Theorem 3, give a generalization of the results from [25] for HetNets.*

Figure 6 shows the relative coverage probability gain of both IA-MRC and IB-MRC over SC for $N = 2$ and $N = 4$. The result for IA-MRC with $N = 4$ was obtained by numerical simulations as Theorem 2 and Corollary 2 treat only the case

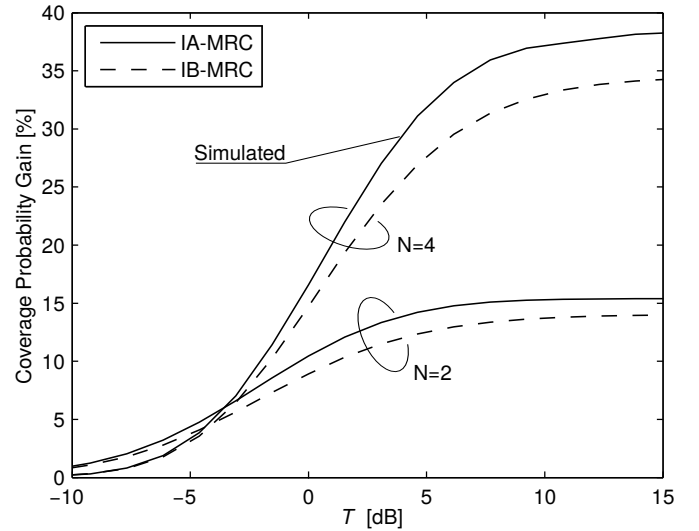


Fig. 6. Relative coverage probability gain of IA-MRC and IB-MRC over SC for $N = 2$ and $N = 4$. Parameters are $\alpha_k \equiv \alpha = 3.7$, $M_k \equiv M = 1$ and $\sigma^2 = 0$.

$N = 2$. As expected, MRC outperforms SC, particularly at large T . However, for practical T around a few dB (which corresponds to between 70-80% covered users), the gap is less than 10% for $N = 2$. Here, the additional complexity associated with MRC might not be justified as SC achieves similar performance. Nevertheless, adding more Rx antennas increases the relative performance (about 25% for $N = 4$ at practical T). This increase is sublinear in N , which is consistent with the literature [37].

VI. CONCLUSION

We developed a stochastic model for analyzing the performance of downlink MIMO diversity with MRC in HetNets using tools from stochastic geometry. We showed that adding more Tx antennas at the BSs increases the coverage probability on the one hand, while it impacts the relative performance of IB-MRC and IA-MRC on the other. One important design insight that arises from our analysis is that IA-MRC is less favorable than IB-MRC when multiple Tx antennas are used. Another key insight is that the full-correlation model provides a reasonably tight approximation for IA-MRC; this could enable the analysis of more sophisticated MIMO techniques, which may be hopeless when considering the exact correlation structure.

Future work may include extending the model to incorporate other linear combining schemes in combination with Tx diversity. Moreover, a performance comparison of the considered MIMO diversity system with more sophisticated MIMO schemes under realistic assumptions, e.g., imperfect CSI-T and/or imperfect interference signal estimation at the receivers, would offer a better understanding of MIMO schemes in HetNets. For instance, this could help finding optimal switching points between different schemes in HetNets.

APPENDIX

A. Proof of Theorem 1

Applying the law of total probability and making use of Lemma 1, we can express (12) by

$$P_c = \sum_{\ell=1}^K A_\ell \int_0^\infty f_{y,\ell}(y) \mathbb{P}(\text{SINR}_\ell(y) \geq T) dy, \quad (39)$$

where $\mathbb{P}(\text{SINR}_\ell(y) \geq T)$ can be seen as the *conditional* P_c , given ℓ, y . With Lemma 2, the conditional P_c can be rewritten as

$$\begin{aligned} \mathbb{P}(\text{SINR}_\ell(y) \geq T) &= \mathbb{P}\left(\|\mathbf{H}_o\|_F^2 \geq \frac{S_\ell T}{P_\ell y^{-\alpha_\ell}} \left(\sum_{k=1}^K \sum_{i \in \Phi_k^o} l_{i,\text{eqv}} + \sigma^2\right)\right) \\ &\stackrel{(a)}{=} \sum_{m=0}^{NM_\ell-1} \frac{(-1)^m}{m!} \mathbb{E}_Y[(-1)^m Y^m e^{-Y}] \\ &\stackrel{(b)}{=} \sum_{m=0}^{NM_\ell-1} \frac{(-1)^m}{m!} \frac{d^m}{ds^m} [\mathcal{L}_Y(s)]_{s=1}, \end{aligned} \quad (40)$$

where in (a) we define $Y \triangleq \frac{S_\ell T}{P_\ell y^{-\alpha_\ell}} (\sum_{k=1}^K \sum_{i \in \Phi_k^o} l_{i,\text{eqv}} + \sigma^2)$ and (b) follows from the differentiation rule for Laplace transforms. With Lemma 3, $\mathcal{L}_Y(s)$ can be obtained as

$$\begin{aligned} \mathcal{L}_Y(s) &= \exp\left(-\frac{s S_\ell T}{\overline{\text{SNR}}_\ell(y)} - \pi \sum_{k=1}^K \lambda_k \hat{P}_k^{2/\alpha_k} y^{2/\hat{\alpha}_k}\right. \\ &\quad \left. \times \left[{}_2F_1\left(-\frac{2}{\alpha_k}, S_k, 1 - \frac{2}{\alpha_k}; -\frac{sT}{S_k}\right) - 1\right]\right), \end{aligned} \quad (41)$$

where $\overline{\text{SNR}}_\ell(y) \triangleq P_\ell y^{-\alpha_\ell} / \sigma^2$ is the average signal-to-noise ratio and $\hat{S}_k \triangleq S_k / S_\ell$. De-conditioning on y and ℓ yields the final result. ■

B. Proof of Theorem 2

With the law of total probability, Lemma 1, and (24), we can rewrite (12) as

$$P_c = \sum_{\ell=1}^K A_\ell \int_0^\infty f_{y,\ell}(y) \mathbb{P}(\text{SINR}_\ell(y) \geq T) dy. \quad (42)$$

Next, we focus on $\mathbb{P}(\text{SINR}_\ell(y) \geq T)$, which after conditioning on Φ^o , yields

$$\begin{aligned} \mathbb{E}_{\Phi^o}[\mathbb{P}(\text{SINR}_1 \geq T - \text{SINR}_2 | \Phi^o)] &= \mathbb{E}_{\Phi^o}\left[\int_0^\infty \mathbb{P}(\text{SINR}_1 \geq T - z | \Phi^o) f_{\text{SINR}_2 | \Phi^o}(z) dz\right], \end{aligned} \quad (43)$$

where we have defined the per-antenna conditional SINR

$$\text{SINR}_n \triangleq \frac{P_\ell}{M_\ell y^{\alpha_\ell}} \frac{\|\mathbf{h}_{o,n}\|_F^2}{l_n + \sigma^2}. \quad (44)$$

Applying the same steps as in (40), $\mathbb{P}(\text{SINR}_1 \geq T - z | \Phi^o)$ inside the integral in (43) can be evaluated as

$$\begin{aligned} \sum_{m=0}^{M_\ell-1} \frac{(-1)^m}{m!} \frac{d^m}{ds^m} \left[\exp\left(-\frac{s M_\ell (T - z)^+}{\overline{\text{SNR}}_\ell(y)}\right) \right. \\ \left. \times \prod_{k=1}^K \prod_{i \in \Phi_k^o} \left(1 + \frac{s (T - z)^+ \hat{P}_k y^{\alpha_\ell}}{\hat{M}_k \|x_i\|^{\alpha_k}}\right)^{-M_k} \right]_{s=1}. \end{aligned} \quad (45)$$

Similarly, we have

$$\begin{aligned} f_{\text{SINR}_2 | \Phi^o}(z) &= \frac{d}{dw} [\mathbb{P}(\text{SINR}_2 \leq w | \Phi^o)]_{w=z} \\ &= \frac{(-1)^{M_\ell}}{z \Gamma(M_\ell)} \frac{d^{M_\ell}}{dt^{M_\ell}} \left[\exp\left(-\frac{t M_\ell z}{\overline{\text{SNR}}_\ell(y)}\right) \right. \\ &\quad \left. \times \prod_{k=1}^K \prod_{x_i \in \Phi_k^o} \left(1 + \frac{t z \hat{P}_k y^{\alpha_\ell}}{\hat{M}_k \|x_i\|^{\alpha_k}}\right)^{-M_k} \right]_{t=1}. \end{aligned} \quad (46)$$

By Fubini's theorem [40], the expectation \mathbb{E}_{Φ^o} can be moved inside the integral over z in (43). By Leibniz integration rule for infinite integrals [36], the differentiations d^m/ds^m in (45) and d^{M_ℓ}/dt^{M_ℓ} in (46) can be moved outside \mathbb{E}_{Φ^o} . Since the Φ_k^o are independent, we then have

$$\begin{aligned} \mathbb{E} \left[\prod_{k=1}^K \prod_{x_i \in \Phi_k^o} \left(1 + \frac{s (T - z)^+ \hat{P}_k y^{\alpha_\ell}}{\hat{M}_k \|x_i\|^{\alpha_k}}\right)^{-M_k} \left(1 + \frac{t z \hat{P}_k y^{\alpha_\ell}}{\hat{M}_k \|x_i\|^{\alpha_k}}\right)^{-M_k} \right] \\ = \exp\left\{-\pi \sum_{k=1}^K \lambda_k \hat{P}_k^{2/\alpha_k} y^{2/\hat{\alpha}_k} \Psi\left(\frac{s}{\hat{M}_k} (T - z)^+, \frac{t z}{\hat{M}_k}, M_k, \alpha_k\right)\right\}, \end{aligned} \quad (47)$$

where $\hat{M}_k \triangleq M_k / M_\ell$ and

$$\Psi(a_1, a_2, p, q) = \int_1^\infty 1 - \left[\left(1 + \frac{a_1}{u^{q/2}}\right) \left(1 + \frac{a_2}{u^{q/2}}\right)\right]^{-p} du. \quad (48)$$

Combining (42) – (47) yields the result. ■

C. Proof of Proposition 1

Recall that in the no-correlation model the interferer locations originate from different point processes, say Φ^o and $\Phi^{o'}$, for each of the two antennas. Then, (47) decomposes to

$$\begin{aligned} \mathbb{E}_{\Phi^o} \left[\prod_{k=1}^K \prod_{x_i \in \Phi_k^o} \left(1 + \frac{s (T - z)^+ \hat{P}_k y^{\alpha_\ell}}{\hat{M}_k \|x_i\|^{\alpha_k}}\right)^{-M_k} \right] \\ \times \mathbb{E}_{\Phi^{o'}} \left[\prod_{k=1}^K \prod_{x_i \in \Phi_k^{o'}} \left(1 + \frac{t z \hat{P}_k y^{\alpha_\ell}}{\hat{M}_k \|x_i\|^{\alpha_k}}\right)^{-M_k} \right] \\ \stackrel{(a)}{=} \exp\left\{-\pi \sum_{k=1}^K \lambda_k \hat{P}_k^{2/\alpha_k} y^{2/\hat{\alpha}_k} \right. \\ \times \left[{}_2F_1\left(-\frac{2}{\alpha_k}, M_k, 1 - \frac{2}{\alpha_k}; -\frac{s}{\hat{M}_k} (T - z)^+\right) - 1 \right. \\ \left. \left. + {}_2F_1\left(-\frac{2}{\alpha_k}, M_k, 1 - \frac{2}{\alpha_k}; -\frac{t z}{\hat{M}_k}\right) - 1\right]\right\}, \end{aligned} \quad (49)$$

where (a) follows from Lemma 3. ■

REFERENCES

- [1] R. Tanbourgi and F. K. Jondral, "Downlink MIMO diversity with maximal-ratio combining in heterogeneous cellular networks," in *IEEE Intl. Conference on Commun.*, 2015, submitted.
- [2] J. G. Andrews *et al.*, "What will 5G be?" *IEEE J. Sel. Areas Commun.*, vol. 32, no. 6, pp. 1065–1082, Jun. 2014.
- [3] Q. H. Spencer, A. L. Swindlehurst, and M. Haardt, "Zero-forcing methods for downlink spatial multiplexing in multiuser MIMO channels," *IEEE Trans. Signal Process.*, vol. 52, no. 2, pp. 461–471, Feb. 2004.
- [4] D. Gesbert *et al.*, "Shifting the MIMO paradigm," *IEEE Signal Process. Mag.*, vol. 24, no. 5, pp. 36–46, Sep. 2007.
- [5] H. S. Dhillon, M. Kountouris, and J. G. Andrews, "Downlink MIMO hetnets: Modeling, ordering results and performance analysis," *IEEE Trans. Wireless Commun.*, vol. 12, no. 10, pp. 5208–5222, Oct. 2013.
- [6] A. K. Gupta, H. S. Dhillon, S. Vishwanath, and J. G. Andrews, "Downlink multi-antenna heterogeneous cellular network with load balancing," *IEEE Trans. Commun.*, vol. 62, no. 11, pp. 4052–4067, Nov. 2014.
- [7] Q. H. Spencer, C. B. Peel, A. L. Swindlehurst, and M. Haardt, "An introduction to the multi-user MIMO downlink," *IEEE Commun. Mag.*, vol. 42, no. 10, pp. 60–67, Oct. 2004.
- [8] 3GPP, "Further advancements for E-UTRA," TR 36.213, Tech. Rep., Mar. 2008.
- [9] D. Tse and P. Viswanath, *Fundamentals of Wireless Communication*. Cambridge University Press, 2005.
- [10] D. G. Brennan, "Linear diversity combining techniques," *Proc. IEEE*, vol. 91, no. 2, pp. 331–356, Feb. 2003.
- [11] T. Benedict and T. Soong, "The joint estimation of signal and noise from the sum envelope," *IEEE Trans. Inf. Theory*, vol. 13, no. 3, pp. 447–454, Jul. 1967.
- [12] D. Pauluzzi and N. Beaulieu, "A comparison of SNR estimation techniques for the AWGN channel," *IEEE Trans. Commun.*, vol. 48, no. 10, pp. 1681–1691, Oct. 2000.
- [13] J. Cui and A. U. H. Sheikh, "Outage probability of cellular radio systems using maximal ratio combining in the presence of multiple interferers," *IEEE Trans. Commun.*, vol. 47, no. 8, pp. 1121–1124, Aug. 1999.
- [14] V. Aalo and C. Chayawan, "Outage probability of cellular radio systems using maximal ratio combining in Rayleigh fading channel with multiple interferers," *Electronics Letters*, vol. 36, no. 15, pp. 1314–1315, Jul. 2000.
- [15] X. Cui, Q. Zhang, and Z. Feng, "Outage performance for maximal ratio combiner in the presence of unequal-power co-channel interferers," *IEEE Commun. Lett.*, vol. 8, no. 5, pp. 289–291, May 2004.
- [16] A. M. Hunter, J. G. Andrews, and S. Weber, "Transmission capacity of ad hoc networks with spatial diversity," *IEEE Trans. Wireless Commun.*, vol. 7, no. 12, pp. 5058–5071, Dec. 2008.
- [17] A. Chopra and B. L. Evans, "Joint statistics of radio frequency interference in multiantenna receivers," *IEEE Trans. Signal Process.*, vol. 60, no. 7, pp. 3588–3603, Jul. 2012.
- [18] R. Tanbourgi, H. S. Dhillon, J. G. Andrews, and F. K. Jondral, "Effect of spatial interference correlation on the performance of maximum ratio combining," *IEEE Trans. Wireless Commun.*, vol. 13, no. 6, pp. 3307–3316, June 2014.
- [19] —, "Dual-branch MRC receivers under spatial interference correlation and Nakagami fading," *IEEE Trans. Commun.*, vol. 62, no. 6, pp. 1830–1844, Jun. 2014.
- [20] —, "Dual-branch MRC receivers in the cellular downlink under spatial interference correlation," in *20th European Wireless Conference*, May 2014.
- [21] D. Stoyan, W. Kendall, and J. Mecke, *Stochastic Geometry and its Applications*, 2nd ed. Wiley, 1995.
- [22] J. G. Andrews, F. Baccelli, and R. K. Ganti, "A tractable approach to coverage and rate in cellular networks," *IEEE Trans. Commun.*, vol. 59, no. 11, pp. 3122–3134, Nov. 2011.
- [23] H.-S. Jo, Y. J. Sang, P. Xia, and J. G. Andrews, "Heterogeneous cellular networks with flexible cell association: A comprehensive downlink SINR analysis," *IEEE Trans. Wireless Commun.*, vol. 11, no. 10, pp. 3484–3495, Oct. 2012.
- [24] H. S. Dhillon, R. K. Ganti, F. Baccelli, and J. G. Andrews, "Modeling and analysis of K -tier downlink heterogeneous cellular networks," *IEEE J. Sel. Areas Commun.*, vol. 30, no. 3, pp. 550–560, Apr. 2012.
- [25] X. Zhang and M. Haenggi, "A stochastic geometry analysis of inter-cell interference coordination and intra-cell diversity," *IEEE Trans. Wireless Commun.*, vol. 13, no. 12, pp. 6655–6669, Dec. 2014.
- [26] M. Haenggi, "Diversity loss due to interference correlation," *IEEE Commun. Lett.*, vol. 16, no. 10, pp. 1600–1603, Oct. 2012.
- [27] M. Haenggi and R. Smarandache, "Diversity polynomials for the analysis of temporal correlations in wireless networks," *IEEE Trans. Wireless Commun.*, vol. 12, no. 11, pp. 5940–5951, Nov. 2013.
- [28] M. Haenggi, *Stochastic Geometry for Wireless Networks*. Cambridge University Press, 2012.
- [29] A. Shah and A. Haimovich, "Performance analysis of maximal ratio combining and comparison with optimum combining for mobile radio communications with cochannel interference," *IEEE Trans. Veh. Technol.*, vol. 49, no. 4, pp. 1454–1463, Jul. 2000.
- [30] E. G. Larsson and P. Stoica, *Space-Time Block Coding for Wireless Communications*, 1st ed. Cambridge University Press, 2008.
- [31] 3GPP, "Further advancements for E-UTRA," TR 36.814, Tech. Rep., Mar. 2009.
- [32] B. Hochwald, T. Marzetta, and V. Tarokh, "Multiple-antenna channel hardening and its implications for rate feedback and scheduling," *IEEE Trans. Inf. Theory*, vol. 50, no. 9, pp. 1893–1909, Sep. 2004.
- [33] A. Paulraj, R. Nabar, and D. Gore, *Introduction to Space-Time Wireless Communications*, 1st ed. Cambridge University Press, 2003.
- [34] V. Tarokh, H. Jafarkhani, and A. Calderbank, "Space-time block codes from orthogonal designs," *IEEE Trans. Inf. Theory*, vol. 45, no. 5, pp. 1456–1467, Jul. 1999.
- [35] Y. Shang, "Space-time code designs and fast decoding for MIMO and cooperative communication systems," Ph.D. dissertation, University of Delaware, 2008.
- [36] F. W. Olver, D. W. Lozier, R. F. Boisvert, and C. W. Clark, *NIST Handbook of Mathematical Functions*, 1st ed. Cambridge University Press, 2010.
- [37] A. Goldsmith, *Wireless Communications*. Cambridge University Press, 2005.
- [38] W. Feller, *An Introduction to Probability Theory and Its Applications*, Vol. 2, 2nd ed. Wiley, Jan. 1971.
- [39] R. Tanbourgi and F. K. Jondral, "Analysis of heterogeneous cellular networks under frequency diversity and interference correlation," *IEEE Wireless Commun. Lett.*, vol. PP, no. 99, pp. 1–1, 2014.
- [40] A. Gut, *Probability: A Graduate Course*, ser. Springer Texts in Statistics. New York, NY: Springer, 2005.